THE JOURNAL OF PHYSICAL CHEMISTRY C

Article

pubs.acs.org/JPCC

Dual Functionality of BODIPY Chromophore in Porphyrin-Sensitized Nanocrystalline Solar Cells

Maheshwar Shrestha,[†] Liping Si,[†] Chia-Wei Chang,[§] Hongshan He,*[,†,‡] Andrew Sykes,[∥] Ching-Yao Lin,[⊥] and Eric Wei-Guang Diau[§]

[†]Center for Advanced Photovoltaics, and [‡]Department of Chemistry and Biochemistry, South Dakota State University, Brookings, South Dakota 57007, United States

[§]Department of Applied Chemistry and Institute of Molecular Science, National Chiao Tung University, Hsinchu 30010, Taiwan

[∥]Department of Chemistry, University of South Dakota, Vermillion, South Dakota 57069, United States

[⊥]Department of Applied Chemistry, National Chi Nan University, Puli, Nantou Hsien 54561, Taiwan

Supporting Information

ABSTRACT: A new organic dye (BET) was synthesized and coadsorbed on TiO_2 nanoparticles to make mixed BET/porphyrin-sensitized solar cells (DSCs). The BET is a boron dipyrromethene compound with one benzoic acid group attached to the meso position for its binding to the TiO_2 nanoparticles and two ethyl groups in the 3 and 3′ positions of pyrrolic units to broaden its absorption. Two ethyl groups are in the cis position, as revealed by its single-crystal X-ray diffraction analysis. The BET exhibits strong absorption in the green light region with an absorption maximum at 528 nm in CH_2Cl_2, which is complementary to the absorption spectrum of porphyrin dyes. When the BET coadsorbs on the TiO_2 nanoparticles with porphyrin dyes (TMPZn and LD12), the power conversion efficiencies increase from 1.09% to 2.90% for TMPZn-sensitized solar cells and from 6.65% to 7.60% for LD12-sensitized solar cells, respectively. The IPCE of the devices in the green light region increases dramatically due to the cosensitizing effect of BET. The fluorescence of BET in solution is partially quenched and that of porphyrin is enhanced in the presence of BET dye, indicating an intermolecular energy transfer from BET to the porphyrin dyes. The direct electron injection from BET to the TiO_2 conduction band was rather poor; only negligible photocurrent was observed. Comparative studies of absorption spectra on the TiO_2 nanoparticle films and electrochemical impedance at the dye/TiO_2 interface also indicate that the BET is an excellent coadsorber to prevent the aggregation of porphyrin dyes. An intermolecular energy transfer model is proposed to account for the observed photovoltaic enhancement of the cosensitization system.

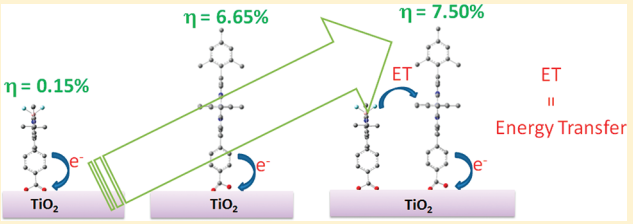

1. INTRODUCTION

Dye-sensitized solar cells (DSCs) are lightweight devices made from inexpensive materials and can be adapted for a variety of indoor and outdoor applications with minimal environmental impact.[1−6] As such, they are a promising technology for the cost-effective conversion of solar energy to electricity. The state-of-the-art DSC is a Grätzel type, titanium dioxide nanoparticles (TiO_2 NPs)-based electrochemical device, in which dye-coated and interconnected TiO_2 NPs in the anatase phase are randomly packed on a substrate, such as fluorine−tin−oxide (FTO)-coated transparent conducting glass (TCO glass).[2] Electrons from dyes in the excited states are injected into the TiO_2 conduction band and transport through a network of interconnected TiO_2 particles to the TCO layer to the external circuit. Nevertheless, the current technology only produces the cells with energy conversion efficiency up to ∼12.3%,[7] which impedes the commercialization of this technology for mass production.

The efficiency of a DSC is determined by many factors, such as structure and absorption capability of the dye, morphology of the TiO_2 nanocrystalline materials, interactions of the dye with the TiO_2, and the electrolyte compositions. Among those factors, the dye plays the most significant role. During the past two decades, numerous ruthenium-based dyes have been examined to reach the efficiency of ∼11%.[6] Alternatively, porphyrins[1,4,8−39] have shown great promise to replace ruthenium-based dyes for cost-effectiveness. Extensive research has revealed that the efficiency of porphyrin-sensitized solar cells can be increased by adding donor groups to the porphyrin ring, attaching bulky substituents to the phenyl groups, or introducing double or triple bonds between the porphyrin ring and the anchoring carboxylic group (COOH). There are two major challenges that need to be overcome. The first one is how to broaden the absorption capability of dyes. The power conversion efficiency of a DSC at each wavelength is the product of light-harvesting efficiency (LHE) of the dye,

Received: October 31, 2011
Revised: April 15, 2012
Published: April 23, 2012

   dx.doi.org/10.1021/jp210458j | J. Phys. Chem. C 2012, 116, 10451−10460

Scheme 1. Schematic of DSCs and Structures of TMPZn, LD12, and BET Dyes[a]

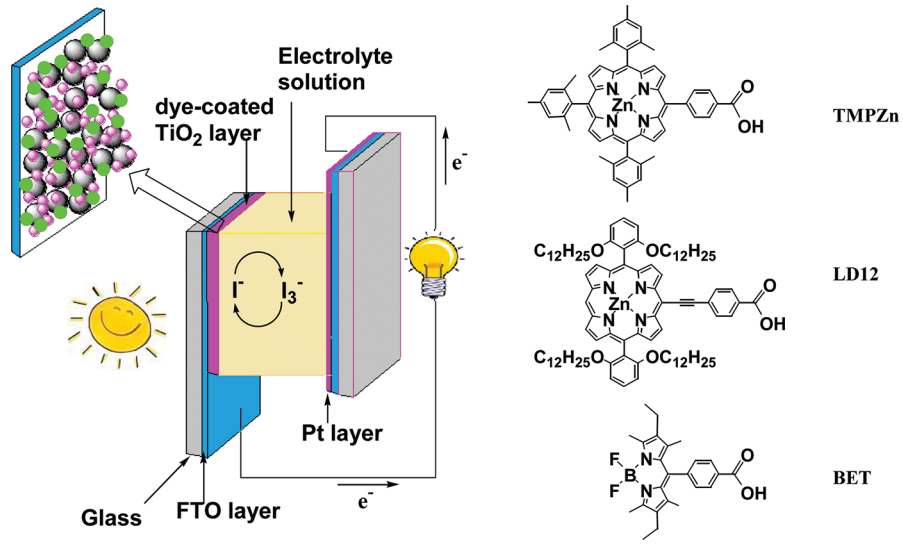

[a]The purple and green dots stand for two different dyes.

electron injection efficiency from the dye to the semiconductor (η_{inj}), and electron collection efficiency of the semiconductor.[12,14,20,27,28,40−44] The LHE is directly linked to how well the absorption spectrum of the dye is matched to the solar spectrum. Most zinc porphyrins exhibit one strong Soret band around 420 nm and two weak Q bands between 550 and 650 nm, with a gap between 450 and 550 nm to match the solar spectrum. A complementary organic dye is usually implemented to make up this spectral mismatch.[16] Grätzel et al. reported[16] that the energy conversion efficiency of the porphyrin YD-2 sensitized solar cells increased from 5.6% to 6.9% when the dye D205 with a complementary absorption in the green light region was used. More recently, Yalla et al.[7] introduced long alkoxyl groups into this porphyrin ring and achieved an unprecedented 12.3% energy conversion efficiency in combination with a cobalt-based electrolyte and a complementary dye Y123. The second challenge is how to reduce the dye aggregation. Reduction of η_{inj} due to aggregation-induced energy transfer becomes a severe problem for the porphyrin dyes because of their planar structural characteristics. A coabsorber, such as chenodeoxycholic acid (CDCA), was usually added during the dye-loading process to separate the porphyrin molecules so that their self-quenching can be minimized.[20,45] However, the addition of a coadsorber and a complementary dye will lower the amount of dye loading of the porphyrins on the TiO_2 surface due to their occupation of binding sites, which ultimately will lower the overall cell efficiency.[46] Therefore, there is a trade-off between the cosensitizer and the coadsorber when both are used to improve the photovoltaic performance of porphyrin-sensitized solar cells. As a result, there is an imperative need for developing a cosensitizer that can also act as a coadsorber. One class of dyes that could be good candidates for this purpose is BODIPY molecules.[47,48]

The BODIPYs are boron dipyrromethene compounds with strong absorption near 500 nm, a region in which the porphyrin dyes usually exhibit very weak absorption. BODIPYs also emit strongly in the green light region with excellent fluorescence quantum yield. As their absorption band is very narrow, the BODIPY-sensitized solar cells display very limited energy conversion efficiencies.[23,47,49−52] In this Article, we will explore the possibility of using a BODIPY dye as a coadsorber and a cosensitizer. The BODIPY dye (BET), as shown in Scheme 1, has the same benzoic acid anchoring group as in the porphyrin dyes (TMPZn and LD12). The alignment of the benzoic acid anchoring group in BET is also very similar to that in porphyrin dyes. In addition, two ethyl groups are attached to the 3 and 3′ positions of the BODIPY core, which could provide steric hindrance to weaken the porphyrin−porphyrin interactions. Our results showed that the BET successfully acted as a cosensitizer and a coadsorber. The cell efficiencies increased from 1.09% to 2.90% and from 6.65% to 7.50% when the TMPZn and LD12 were, respectively, cosensitized with BET, whereas the device made of BET alone showed negligible energy conversion efficiency. This significant enhancement on cell performance is attributed to the complementary absorption of sunlight by the BET and the reduced porphyrin aggregation. Reported here are their synthesis, photophysical properties, and photovoltaic performances.

2. EXPERIMENTAL SECTION

General. All solvents were reagent grade and distilled under N_2 prior to use. Chenodeoxycholic acid (CDCA), methyl-4-formyl-benzoate, mesitaldehyde, and 2,4-dimethyl-3-ethyl-1*H*-pyrrole were obtained commercially and used without further purification. Other chemicals were analytical grade and used as received. 5−4-Carboxylphenyl-10,15,20-tri(2,3,5-trimethylphenyl)porphyrin (TMPZn) and LD12 were synthesized according to a method reported previously.[10,20]

Absorption spectra were performed on an Agilent HP 8453 UV−vis spectrophotometer using a 1.0 cm quartz cuvette. Steady-state fluorescence spectra were obtained on a FS920 spectrophotometer (Edinburgh Instrument, Inc.) with an arc lamp (Xe900) as light source and an Hamamatsu R928P as an emission monitor. A 1.0 cm quartz cuvette was used for all measurements. The emission spectra were recorded between 450 and 745 nm with excitation wavelength at 375 nm.

Synthesis of the BET. The BET was prepared from 2,4-dimethyl-3-ethyl-1*H*-pyrrole and 4-formybenzoic acid in a one-pot reaction. To a dry CH_2Cl_2 solution (100 mL) were added

dx.doi.org/10.1021/jp210458j | J. Phys. Chem. C 2012, 116, 10451−10460

2,4-dimethyl-3-ethyl-1*H*-pyrrole (0.50 g, 4.1 mmol) and 4-formybenzoic acid (0.30 g, 2.0 mmol) under nitrogen atmosphere. One drop of trifluoroacetic acid was added to initiate the reaction. The resulting mixture was stirred for 12 h at room temperature. The color of the solution changed gradually from slight yellow to dark brown. Next, dichlorodicyanobenzoquinone (DDQ) (0.45 g, 2 mmol) in CH_2Cl_2 (10 mL) was added. The color of the solution immediately changed to purple. After continued stirring for 30 min, triethylamine (4 mL) and $BF_3{\cdot}OEt_2$ (4 mL) were added consecutively. The color of the solution became dark purple, and green fluorescence was observed under UV lamp (365 nm). It was stirred for another 6 h, and then the solution was passed through a short column filled with silica to remove the black and reddish impurities. The solvent was reduced to ∼5 mL and loaded on a silica gel for purification. Chloroform was used as the eluting solvent. After two consecutive columns, the final red product was obtained by recrystallization from CH_2Cl_2/methanol. Yield: 0.41 g, 49%. ^{1}H NMR ($CDCl_3$): 8.08 (d, 2H), 7.3 (d, 2H), 2.42 (s, 6H), 2.15 (dd, 4H), 1.11 (s, 6H), 0.79 (t, 6H).

Single-Crystal X-ray Diffraction Analysis. Single crystals were obtained by slow evaporation of dichloromethane−methanol solution of the BET for 1 week at room temperature. The crystal was mounted on a glass fiber before data collection. Diffraction measurements were made on a Bruker APEC II CCD detector at 293(2) K. The frames were collected with a scan width of 0.3° in ω and integrated with Bruker SAINT Software package using a narrow-frame integration algorithm. The unit cell was determined by least-squares upon the refinement of *XYZ*-centroids of reflections above 20$\sigma(I)$. The data were corrected for absorption using the SADABS program. The structures were refined on F^2 using the Bruker SHELXTL[53] (version 5.1) software package. Crystal data for BET: $C_{24}H_{27}BF_2N_2O_2$, MW = 424.29, monoclinic, space group = $P2(1)/n$, a = 11.476(4), b = 9.273(3), c = 20.633(6) Å, β = 100.833(4)°, V = 2156.5(11) Å^3, Z = 4, ρ_{calcd} = 1.307 Mg m^{-3}, μ (Mo Kα) = 0.094 mm^{-1}, $F(000)$ = 896, T = 293 (2) K. 19 993 reflections were measured, of which 5994 were unique (R_{int} = 0.0689). Final R_1 = 0.0563 and wR_2 = 0.1557 values were obtained for 2497 observed reflections with $I > 2\sigma(I)$, 284 parameters, and GOF = 1.052.

Dye Loading Kinetics and Dye Loading Density. The dye loading densities were obtained by monitoring changes of the absorbance of TMPZn and BET in methanol in a 1.0 cm cuvette in the presence of TiO_2 film. The TiO_2 film on a small piece of microscope glass slide was prepared using a method similar to cell fabrication. The film was placed at the bottom of the cuvette. The cuvette was sealed, and the absorption spectrum was recorded every 10 min. The mole number of dye molecules adsorbed on the TiO_2 surface (Q_t, mol/cm^2) at time t (min) was calculated using the following equation:[54−56]

$$Q_t = \frac{(C_0 - C_t) \times V}{m \times A}$$

where C_0 is the initial concentration of dye solution, C_t is the concentration of the dye solution at the time t, m is the weight of the TiO_2 film, V is the total volume of the solution, and A is the surface area of the TiO_2 nanoparticles (70 cm^2/g). The amount of adsorbed dye on the TiO_2 film at equilibrium (Q_e) was obtained by fitting the data using the pseudo first-order model:

$$Q_t = Q_e - Q_e e^{-kt}$$

where k (min^{-1}) is the first-order adsorption constant.

Fabrication and Characterization of DSCs. The commercial nanocrystalline TiO_2 paste from the Dyesol (DSL-18NRT) was coated on a commercial fluorine−tin−oxide (FTO) using the doctor-blade method. After air-drying for about 30 min, the sample was put into an oven for sintering (500 °C for 30 min) in ambient oxygen. The sample was then cooled to room temperature and was immersed in a $TiCl_4$ aqueous solution (20 mM) for 1 h. The film was air-dried and sintered again at 500 °C for 30 min. The film was then put into the dye solution (∼0.2 mM in methanol) at room temperature and kept for 1 h to obtain better efficiency. The film was taken out, flushed with methanol, and vacuum-dried for 1 h. The thickness of the film was ∼13 μm from cross-view images of scanning electron microscope (SEM). The counter-electrode was prepared by sputtering a 16 nm-thick film of the Pt on the FTO glass. A mask made from the Parafilm was used as a spacer for two electrodes and sealing material. The electrolyte solution was injected from two precut channels in the mask. The outside of the final cell was sealed by hot glue. The electrolyte is an acetonitrile solution having 0.6 M 1-propyl-2,3-dimethylimidazolium iodide, 0.05 M I_2, 0.1 M LiI, 0.1 M guanidine thiocynate, and 0.5 M *tert*-butylpyridine. The active area of the cell was 0.16 cm^2. The solar cells thus prepared were characterized for the current−voltage measurements using a standard light source (xenon arc lamp) with light intensity of 100 mW/cm^2 under AM 1.5G conditions. The fill factor (FF) and overall energy conversion efficiency (η) were calculated by η (%) = $P_{max} \times 100/(P_{in} \times A)$ and FF = $P_{max}/(J_{SC} \times V_{OC})$, where P_{max} is the maximum output power of the cells, P_{in} is the power density of the light source, J_{sc} is the short-circuit current density, V_{OC} is the open-circuit voltage, and A is the active area of the cell.

IPCE and EIS Measurements. Incident photon to charge carrier efficiency (IPCE) experiments were performed on an Agilent semiconductor parameter analyzer with an Xe arc lamp and an Newport monochromator. Monochromatic light was incident on the sample through focusing lenses. The National Renewable Energy Laboratory (NREL) calibrated photodetector was used as a reference. The samples were scanned from 350 to 850 nm, and the voltage was recorded. The IPCE was calculated using the equation IPCE = (sample voltage × reference voltage)/reference IPCE. The reference IPCE was supplied by the NREL calibrated DSSC under AM1.5 photon flux.

Electrochemical impedance spectroscopy (EIS) measurements were performed on an HP 4192A LF impedance analyzer (5 Hz-13 MHz) in a two-electrode configuration. A 10 mV of AC perturbation was applied ranging between 5 and 10^5 Hz. The measurements were performed in dark under forward bias 0.55 V. A simplified Randle's model was used to fit the data to extract the series resistance (R_S), which accounts for the transport resistance of TCO, the combined charge transfer resistance for electron recombination at the TCO/electrolyte and TiO_2/electrolyte interface (R_{ct}), and the constant phase element representing capacitance at the TCO/electrolyte/TiO_2 interface (CPE1).

3. RESULTS AND DISCUSSION

The TMPZn was synthesized by the condensation between methyl-4-formylbenzoate, mesitaldehyde, and pyrrole, followed by the hydrolyzation in the presence of KOH in THF. The

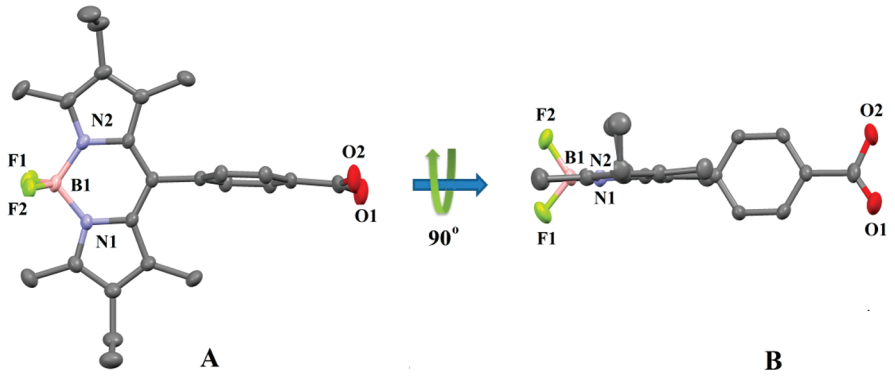

Figure 1. ORTEP diagram of the BET dye with 50% thermal ellipsoid probability. Selected bond lengths (Å): F1−B1 = 1.399(4), F2−B1 = 1.378(4), N1−B1 = 1.537(4), N2−B1 = 1.538(4). Selected bond angles (deg): N1−B1−N2 = 107.1(2).

TMPZn is a purple solid and soluble in most organic solvent including ethanol and methanol. The BET was also prepared by a "one-pot" reaction between 4-formylbenzoic acid and 2,4-dimethyl-3-ethyl-1*H*-pyrrole in CH_2Cl_2, followed by oxidation by the DDQ, deprotonation by NEt_3, and insertion of BF_2 unit by $BF_3{\cdot}OEt_2$ under N_2 atmosphere. The obtained compound has a deep orange color in solid state, yellowish color in CH_2Cl_2, and green color in ethanol. The TMPZn and the BET were characterized by ^1H NMR (see Figure S1). The structure of the BET was also ascertained by the single-crystal X-ray diffraction analysis; the thermal ellipsoid diagram is shown in Figure 1. The BODIPY core structure is very similar to its analogues.[57,58] The benzoic acid group is almost perpendicular to the BODIPY core plane with a dihedral angle of ~78°. This alignment is very similar to that of the mesityl groups, which are rotated perpendicular to the planes of the porphyrin rings. The two ethyl groups at 3 and 3′ positions bend to the same side of the BODIPY core plane. It should be mentioned that the molecules are packed "head to toe" with the formation of an intermolecular hydrogen bond between O1 and F1 in its single-crystal structure.

The absorption and the fluorescence spectra were first acquired in solution at room temperature to gain a basic understanding of their photophysical characteristics. The data for the TMPZn are consistent with other porphyrins reported in the literature. It exhibits a strong absorption peak centered at 424 nm and two weak absorption peaks at longer wavelengths. The BET only shows one narrow absorption peak at 528 nm. As shown in Figure 2, the absorption spectra of the TMPZn and the BET are complementary. The solvent did not exhibit a significant impact on the absorption and the fluorescence of the TMPZn, while a strong solvation effect was observed for the BET. The TMPZn and the BET both exhibited fluorescence under the UV and visible light excitation (Table 1). The TMPZn emitted at ~605 and 656 nm with a decay lifetime of ~2.5 ns. The BET emitted at ~540 nm with a decay lifetime of ~4.5 ns.

As the photovoltaic performance of a cell is highly correlated to the dye loading density on the TiO_2 nanoparticles, we then monitored the adsorption process of the TMPZn and the BET on the TiO_2 nanoparticles and determined their loading density. As shown in Figure 3, the dye loading of the TMPZn was completed within 1 h, whereas the adsorption of BET lasted much longer. The calculated dye loading densities of the BET and the TMPZn were 1.60×10^{-10} and 1.24×10^{-10} mol/cm^2, respectively, which is consistent with their different size. When the BET was added into the TMPZn solution, the dye

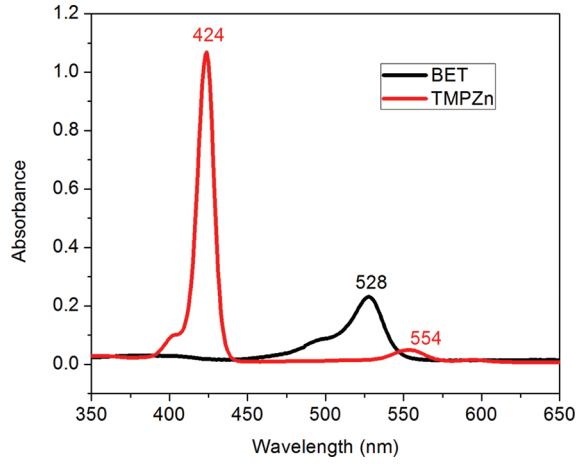

Figure 2. Absorption spectra of the TMPZn and the BET in CH_2Cl_2 at room temperature. The concentration of dyes was 2×10^{-6} mol/L.

Table 1. Absorption and Fluorescence Data of TMPZn and BET at Room Temperature

solvent	dye	absorption λ (nm), ε (M^{-1} cm^{-1})	fluorescence λ (nm), τ (ns)
CH_2Cl_2	TMPZn	424 (5.3×10^5), 554 (2.5×10^4)	604, 656 (2.50)
	BET	528 (1.2×10^5)	543 (4.37)
MeOH	TMPZn	423 (9.5×10^5), 558 (3.0×10^4)	602, 658 (2.48)
	BET	523 (8.14×10^4)	538 (5.37)

loading density of the TMPZn at equilibrium decreased with the increase of TMPZn/BET ratio; however, the total dye loading densities (TMPZn and BET) were almost constant, indicating the surface of TiO_2 nanoparticles was fully covered by dyes in 1 h.

The photovoltaic performances of the DSCs for TMPZn cosensitizing with BET were studied. A typical "sandwich" configuration of the DSC was adapted for this investigation. The results are listed in Table 2. The *J*−*V* curves of these cells are also depicted in Figure 4. The dye loading time was fixed to 1 h as efficiency decreased when the dye-loading time increased from 1 to 5 h. This is consistent with the report from Imahori.[20] The TMPZn-sensitized solar cell gave an energy conversion efficiency of 1.09%, while the BET-sensitized solar cell showed efficiency that is less than 0.1%. When different amounts of BET were added to the TMPZn solution during the dye-loading process, the efficiency of the resulting cells increased

dx.doi.org/10.1021/jp210458j | *J. Phys. Chem. C* 2012, 116, 10451−10460

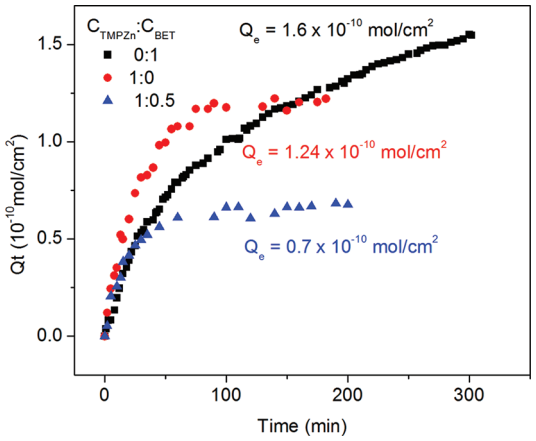

Figure 3. Typical adsorption profile of TMPZn, BET, and TMPZn/BET (molar ratio 1:1) mixture on TiO_2 NP surface in methanol at room temperature. The absorbed amounts of TMPZn and BET on TiO_2 film were determined by measuring the absorbance change at 558 and 523 nm, respectively.

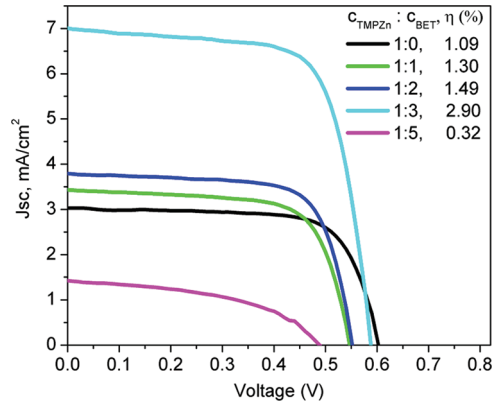

Figure 4. The $J-V$ curves of the DSCs with different molar ratios of TMPZn and BET. The dye loading of the TiO_2 nanoparticle film was carried out in methanol for 1 h.

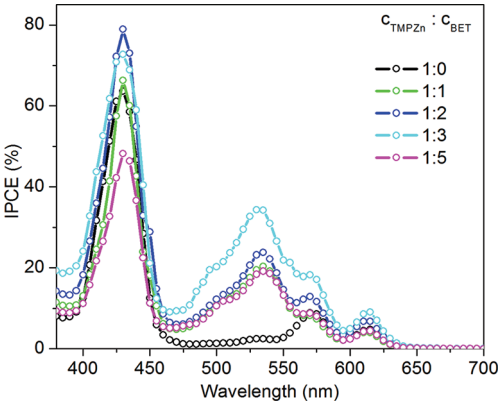

Figure 5. The IPCE curves of the DSCs with different molar ratios of TMPZn and the BET. The same cells used for $J-V$ measurements were used directly for the IPCE measurement.

gradually to 2.90% when the molar ratio of TMPZn/BET reached 1:3. It then decreased to 0.32% when the molar ratio increased to 1:5. A similar trend was also observed for the J_{SC} of the cells; however, the addition of the BET to the TMPZn solution lowered the V_{OC}. The obtained energy conversion efficiency was consistent with the IPCE spectra shown in Figure 5. The IPCE spectra of the TMPZn/BET devices were very similar to the combined absorption spectra of TMPZn and BET. The IPCE values at the Soret region (~350 to 450 nm) increased from 62% (TMPZn/BET, 1:0) to 78% (TMPZn/BET, 1:2) at 424 nm, and then decreased to 47% (TMPZn/BET, 1:5). The IPCE in the Q-band region increased when the molar ratio of TMPZn/BET increased from 1:0 to 1:3. A significant enhancement was observed in the region corresponding to the absorption of the BET. When the molar ratio of the TMPZn/BET increased to 1:5, the IPCE decreased to a level that is still much higher than that of cell with TMPZn alone.

These results showed clearly that BET/TMPZn cosensitized solar cells exhibited more efficient sunlight absorption and electron generation in the green light region. Therefore, the BET is a very good cosensitizer for porphyrin-sensitized solar cells. The question is how this happens. To answer this question, a BET-sensitized solar cell was fabricated under the same conditions. The loading of the BET on the TiO_2 nanoparticles was excellent; however, the energy conversion efficiency was extremely low. Its IPCE spectrum was almost flat from 400 to 700 nm with a small signal around 530 nm. The poor photovoltaic performance of BODIPY dye-sensitized solar cells was also observed in several other reports,[49,59] which could be due to the quick back electron transfer from TiO_2 to the oxidized BET. The significant IPCE enhancement at ~530 nm in BET/TMPZn sensitized solar cell indicated strongly that direct injection of electron to the TiO_2 conduction band, which is normally in cosensitized solar cells, is not the major pathway for electron generation in TMPZn/BET system. Instead, a Föster resonance energy transfer (FRET) from BET to TMPZn is likely to happen. FRET is an energy transfer process[60] in which a donor chromophore in an excited electronic state transfers its excitation energy to a nearby acceptor chromophore in a nonradiative fashion through long-range dipole−dipole interactions. FRET often requires that the fluorescence emission spectrum of the donor molecule must

Table 2. Photovoltaic Parameters of DSCs with Different Molar Ratio of TMPZn and BET[a]

						dye loading density (mol/cm^2)	
entry	[TMPZn]/[BET]	J_{SC} (mA/cm^2)	V_{OC} (V)	FF	η (%)	TMPZn	BET
1	0:1	0.20	0.382	0.478	0.03	0	1.60×10^{-10}
2	1:0	3.25	0.596	0.566	1.09	1.24×10^{-10}	0
3	1:1	3.43	0.546	0.693	1.30	0.343×10^{-10}	0.160×10^{-10}
4	1:2	3.79	0.552	0.714	1.49	0.231×10^{-10}	0.434×10^{-10}
5	1:3	7.00	0.586	0.708	2.90	0.114×10^{-10}	0.450×10^{-10}
6	1:5	1.42	0.488	0.473	0.32	2.28×10^{-13}	0.672×10^{-10}

[a]The dye loading was carried out in methanol for 1 h for cell fabrication.

dx.doi.org/10.1021/jp210458j | J. Phys. Chem. C 2012, 116, 10451−10460

overlap the absorption or excitation spectrum of the acceptor chromophore, in close proximity to one another (typically 1−10 nm), and sufficient fluorescence lifetime of the donor molecule. The FERT process has been widely used in biological system for protein−protein interactions.[60] Recently, it was also observed in dye-sensitized solar cells.[61−71] In the current TMPZn/BET system, BET acts as a donor, whereas TMPZn as an acceptor. More importantly, the fluorescence spectrum of BET and absorption spectrum of TMPZn, as shown in Figure 6A, are significantly overlapped, which provides a high

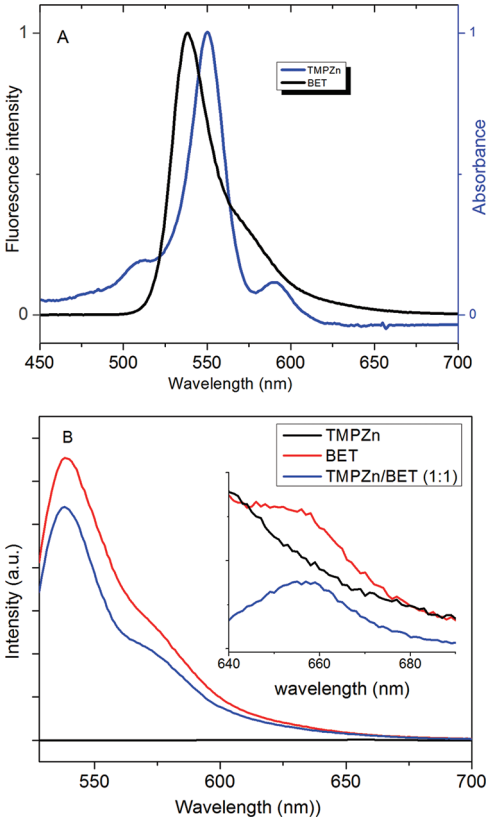

Figure 6. (A) Normalized absorption spectrum of TMPZn and fluorescence spectrum of BET in methanol. (B) The fluorescence spectra of TMPZn, BET, and TMPZn/BET (1:1) in methanol with excitation at 523 nm. The inset is the fluorescence spectra with excitation at 375 nm. The concentration of the two dyes was 8×10^{-6} mol/L.

probability that the FRET process happens. In addition, changes of fluorescence intensity of BET and TMPZn after addition of BET to TMPZn solution also supported this energy transfer mechanism. Figure 6B shows the fluorescence spectra of BET, TMPZn, and TMPZn/BET (1:1 molar ratio). Two wavelengths (375 and 523 nm) were selected to excite TMPZn and BET, respectively. When TMPZn/BET was excited at 523 nm, the emission intensity of BET decreased as compared to that of BET alone. When sample was excited at 375 nm, the emission intensity of TMPZn increased as compared to TMPZn alone. This showed that energy transferred from BET to TMPZn. Considering the distance between BET and TMPZn is very short (estimated to be less than 1.5 nm from single-crystal structures of porphyrin and BET), the energy transfer will be very fast as the rate of energy transfer is proportional to r^{-6}, where r is the distance between BET and TMPZn.[60] The long lifetime of BET (4.5 ns in solution) will be sufficient enough for efficient FRET process.

The enhanced device performance of the BET/TMPZn-sensitized solar cell could also come from the reduced degree of dye aggregation. It is well-known that porphyrins tend to aggregate on the surface of TiO_2 nanoparticles. The introduction of bulky alkyl groups could suppress this effect to some extent; however, a coadsorber, such as CDCA, is widely used to improve cell performance. Grätzel et al. added CDCA to a bulky zinc porphyrin YD-2, and an efficiency of 11% was obtained.[15] The degree of aggregation can be probed by the changes of Soret band of porphyrins adsorbed on the TiO_2 films.[39] Figure 7 shows the absorption spectra of TiO_2

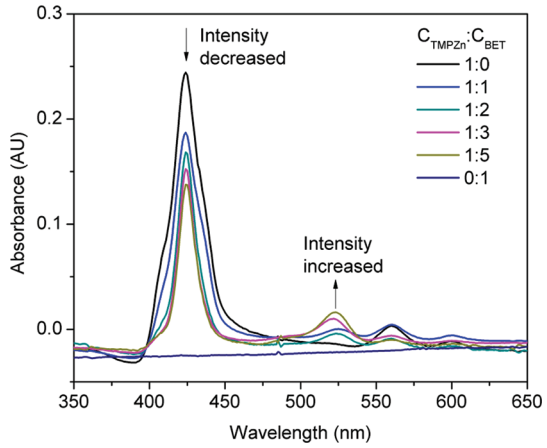

Figure 7. Absorption spectra of the TMPZn on the TiO_2 film in the presence of BET. The dye loading was performed in methanol, whereas the spectra were taken in acetonitrile.

films that were coated with TMPZn and BET under different molar ratios. The experiments were conducted under the same conditions as those for cell fabrication. The TMPZn-coated TiO_2 film gave an absorption spectrum that was similar to its solution sample. The TiO_2 films that were coated by different molar ratios of TMPZn/BET exhibited absorption spectra that were the combination of spectra of two dyes in solution. When the molar ratio of TMPZn/BET increased from 1:0.5 to 1:5, the peak intensities centered at 525 nm increased, whereas that at 425 increased first and then remained almost constant. The Soret band narrowed when the TMPZn/BET ratio increased, which indicated that the BET prevented porphyrin from its aggregation. To further support this conclusion, TMPZ, TMPZn/BET (molar ratio 1:3), and TMPZn/CDCA (molar ratio 1:3)-sensitized solar cells were fabricated and tested under same conditions. The $J-V$ curves are shown in Figure 8, and detailed photovoltaic parameters are listed in Table 3. The increased J_{SC}, V_{OC}, and FF were observed in TMPZn/BET- and TMPZn/CDCA-sensitized cells. The TMPZn/BET-sensitized cell exhibited higher J_{SC} and lower V_{OC} as compared to the TMPZn/CDCA-sensitized cell. The higher current density in the TMPZn/BET-sensitized cell mainly came from the cosensitizing effect of BET through the aforementioned energy transfer mechanism, which did not exist in the TMPZn/CDCA-sensitized cell. The lower open-circuit voltage of the TMPZn/BET-sensitized cell might be due to the effect of charge recombination, for which the TMPZn/CDCA device has less effect. It should be noted that the addition of the BET to the TMPZn during the dye loading process could also

dx.doi.org/10.1021/jp210458j | J. Phys. Chem. C 2012, 116, 10451−10460

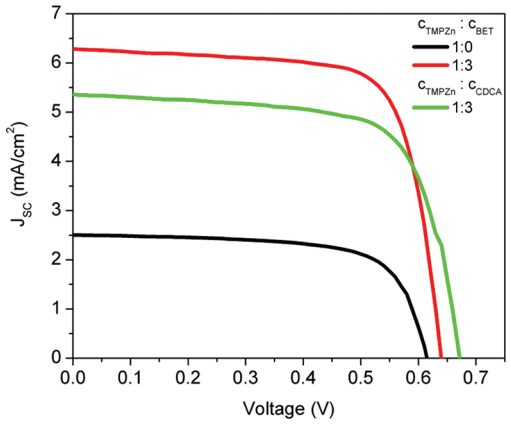

Figure 8. The *J*–*V* curves of DSCs with different molar ratios of TMPZn, BET, and CDCA. The dye loading was carried out in methanol for 1 h.

Table 3. Photovoltaic Parameters of the DSCs with Different Molar Ratios of TMPZn, BET, and CDCA[a]

entry	dye ratio	J_{SC} (mA/cm^2)	V_{OC} (V)	FF	η (%)
1	[TMPZn]/[BET] [1:0]	2.50	0.614	0.688	1.05
2	[TMPZn]/[BET] [1:3]	6.28	0.639	0.726	2.93
3	[TMPZn]/[CDCA] [1:3]	5.36	0.671	0.694	2.51

[a]The dye loading was carried out in methanol for 1 h. The TiO_2 NP-coated TCO glass used for these three cells was from a batch that was different from that used for cells in Table 2.

reduce the aggregation of BET, which was not observed in the BET/CDCA (molar ratio, 1:3)-sensitized solar cell.

To further reveal the function of the BET in the TMPZn/BET-sensitized solar cells, we carried out two sets of electrochemical impedance spectroscopy (EIS) experiments. The EIS is a very useful tool to study the interfacial electron-transport behaviors of the devices.[72−77] The measurements were performed between 5 Hz and 100 kHz, and Randle's model[78] was used to fit the data, as shown in Figure 9. In this model, R_S is the series resistance accounting for transport resistance of TCO; R_{ct} is the combination of charge transfer resistance for electron recombination at the TiO_2/electrolyte interface; while CPE1 is the constant phase element representing capacitance at the TiO_2/electrolyte/interface. The model was found to provide a good fit to the experimental data. In the first set of experiments, the EIS values of solar cells that were sensitized by TMPZn/BET with different molar ratio were measured. The Nyquist plots at applied bias −0.55 V are shown in Figure 9. From these plots, the R_s, R_{ct}, and CPE1 were extracted for all cells. The calculated values of charge transfer resistance are 1534.5, 1549.5, 1136.6, 816.44, and 966.37 Ω for cells with molar ratio TMPZn/BET from 1:0, 1:1, 1:2, 1:3, and 1:5, respectively, indicating that the addition of BET indeed reduced the recombination resistance. In the second set of experiments, the EIS values of cells that were sensitized by TMPZn, TMPZn/CDCA (1:3), and TMPZn/BET (1:3) were measured. The Nyquist plots at applied bias −0.55 V are shown in Figure 10. The R_{ct} values decreased from TMPZn, TMPZn/CDCA, to TMPZn/BET. This indicated similar effects of BET and CDCA on the TMPZn-sensitized solar cells.

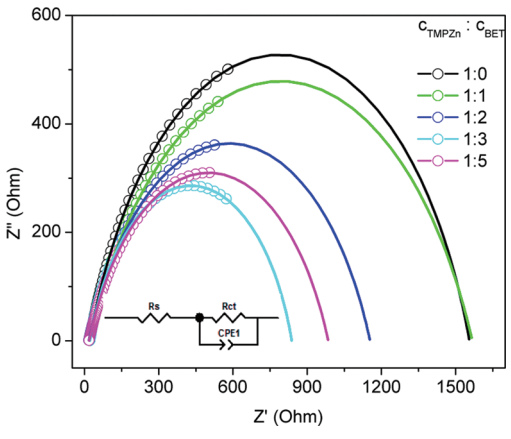

Figure 9. Nyquist plots of the EIS of DSCs that were sensitized by TMPZn and BET with different molar ratios under bias of −0.55 V. The dyeing was carried out in methanol for 1 h. Inset is the equivalent Randle's circuit impedance model used for data fitting. The dots are experimental data; the solid lines are fitting results from Randle's model.

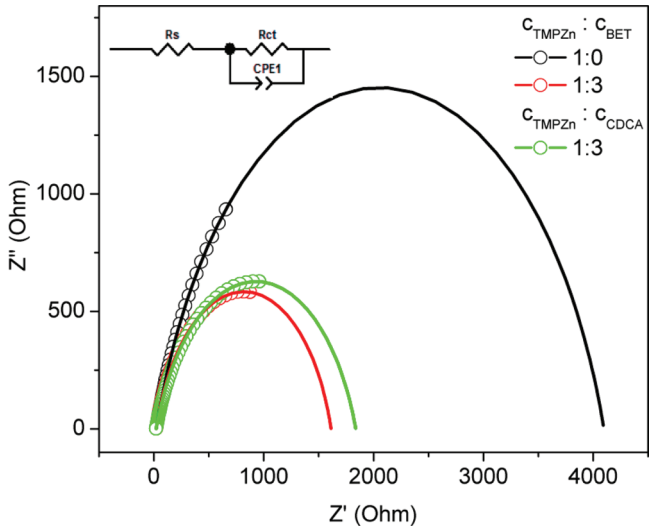

Figure 10. Nyquist plots of the EIS of DSCs that were sensitized by TMPZn, TMPZn/BET (1:3), and TMPZn/CDCA (1:3) under bias of −0.55 V. The dyeing was carried out in methanol for 1 h. Inset is the equivalent Randle's circuit impedance model used for fitting the EIS data. The dots are experimental data; the solid lines are fitting results from Randle's model.

On the basis of these studies, we propose that the TMPZn and the BET are anchored on the TiO_2 surface with the BET located most likely between the TMPZn molecules, as shown in Scheme 2. In the absence of BET, the TMPZn aligns closely on the TiO_2 surface, which leads to significant aggregation of the TMPZn; as a result, electron injection efficiency to the TiO_2 conduction band is reduced. When the BET is added, it inserts between the TMPZn molecules and binds to the TiO_2 surface. The BET acts as a spacer to separate the TMPZn molecules for aggregation. The BET core plane is likely parallel to the porphyrin ring. Because of their structural planarity, the distance between BET and TMPZn will be very short, which will facilitate efficient Föster resonance energy transfer from the BET to the TMPZn followed by a rapid electron injection from TMPZn to the TiO_2 conduction band. A detailed ultrafast

dx.doi.org/10.1021/jp210458j | J. Phys. Chem. C 2012, 116, 10451−10460

Scheme 2. Proposed Alignments of Porphyrin Dye and BET on the Surface of TiO_2 and Energy Transfer Pathway

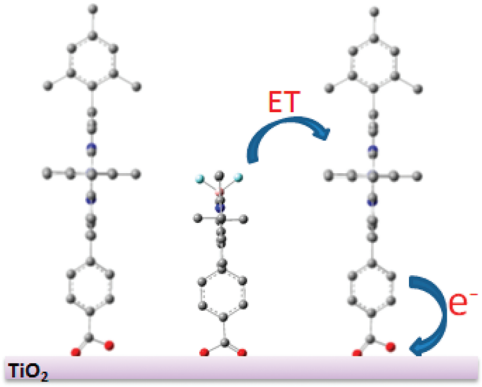

spectroscopic study of this energy transfer process is underway and will be reported in due course.

Finally, we applied BET to one high performance porphyrin dye, LD12,[9] to further demonstrate its promise in achieving high efficiency in DSCs. LD12 is a phenylethynyl functionalized zinc porphyrin with four long alkoxyl chains in the meso position of two phenyl groups. Similar to TMPZn dye, LD12 also exhibits weak absorption in the green light region. Under the same conditions, the LD12-sensitized solar cell exhibited 6.65% conversion efficiency of solar energy to electricity. The LD12/BET-sensitized solar cell exhibited 7.50% energy conversion efficiency. The current−voltage characteristics were shown in Figure 11A, and the corresponding photovoltaic parameters are summarized in Table 4. A significant increase in J_{SC} and a minor decrease in V_{OC} were observed in the LD12/BET system. Notably, the photons in the green region (480−560 nm) were uptaken by BET and converted to the electrons efficiently. The IPCEs of the BET and the LD12 devices at ∼500 nm were ∼5% and ∼40%, respectively, but that of the LD12/BET device was enhanced to ∼70%, as shown in Figure 11B. Such dramatic enhancement was also observed in a BODIPY-functionalized porphyrin dye, where linkage of a BODIPY unit to porphyrin through a triple bond increased the energy conversion efficiency from 0.84% to 1.55%.[23] As compared to its elaborative organic synthesis of this dye, direct use of BODIPY as we proposed in this study provides more benefits for the design of more efficient and cost-effective devices.

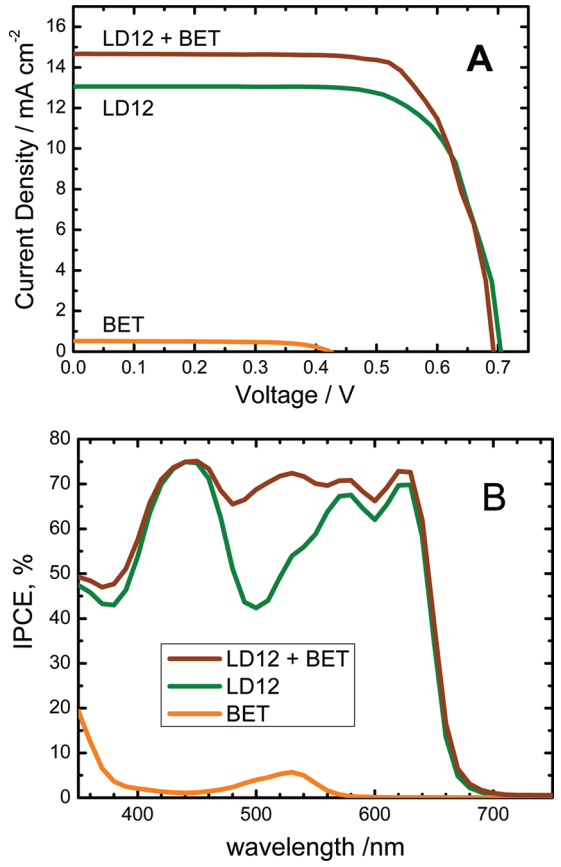

Figure 11. The $J-V$ curves (A) and IPCE (B) of LD12, LD12/BET, and BET-sensitized solar cells.

Table 4. Photovoltaic Parameters of LD12-Sensitized Solar Cells in the Presence of BET[a]

dye	soaking time (h)	J_{SC} (mA/cm^2)	V_{OC} (V)	FF	η (%)
LD12	4	13.066	0.713	0.714	6.65
BET	1	0.523	0.425	0.671	0.15
LD12+BET	4 + 1	14.661	0.705	0.726	7.50

[a]The dye loading was carried out in ethanol. The cells were fabricated and tested as described elsewhere.[9]

4. CONCLUSIONS

A new BODIPY dye (BET) was synthesized and coadsorbed on titanium dioxide nanoparticles to make BET/porphyrin dye-sensitized solar cells. The power conversion efficiencies of the devices increased from 1.09% to 2.90% and from 6.65% to 7.50% when the BET was used as cosensitizer in TMPZn- and LD12-sensitized solar cells, respectively. The BET functions as a cosensitizer due to its strong absorption in the green light region, which is complementary to the absorption of TMPZn and LD12. This is confirmed by the enhanced IPCE between 450 and 650 nm. The BET also functions as a coadsorber, which was supported by the narrowing of the absorption band of the porphyrin on a TiO_2 film in the presence of the BET. Similar recombination resistances at the TiO_2/electrolyte interface for the TMPZn-sensitized solar cells were observed when the BET and chenodeoxycholic acid (CDCA) were used during the dye-loading process. An intermolecular energy transfer mechanism was proposed to explain the observed J_{SC}-enhanced phenomena. The results demonstrate for the first time the dual functionality of BET as an efficient coadsorber in porphyrin-sensitized solar cells and its promise for efficient and cost-effective devices.

■ ASSOCIATED CONTENT

Supporting Information

Complete author lists of refs 8, 29, 30, 38, and 76. This material is available free of charge via the Internet at http://pubs.acs.org.

■ AUTHOR INFORMATION

Corresponding Author

*Tel.: (605) 688-6962. Fax: (605) 688-4401. E-mail: Hongshan.he@sdstate.edu.

Notes

The authors declare no competing financial interest.

■ ACKNOWLEDGMENTS

This research was supported by the National Science Foundation/EPSCoR, Grant No. 0903804, South Dakota State University Research and Scholar Fund (No. 334578). We are grateful to reviewers' and editors' valuable comments that improved this manuscript.

■ REFERENCES

(1) Grätzel, M. *Inorg. Chem.* **2005**, *44*, 6841−6851.
(2) O'Regan, B.; Grätzel, M. *Nature* **1991**, *353*, 737−740.
(3) Henry, J. S. *Adv. Funct. Mater.* **2010**, *20*, 13−19.
(4) Martinez-Diaz, M. V.; de la Torre, G.; Torres, T. *Chem. Commun.* **2010**, *46*, 7090−7108.
(5) He, H.; Dubey, M.; Zhong, Y.; Shrestha, M.; Sykes, A. G. *Eur. J. Inorg. Chem.* **2011**, *25*, 3731−3738.
(6) Grätzel, M. *Acc. Chem. Res.* **2009**, *42*, 1788−1798.
(7) Yella, A.; Lee, H.-W.; Tsao, H. N.; Yi, C.; Chandiran, A. K.; Nazeeruddin, M. K.; Diau, E. W.-G.; Yeh, C.-Y.; Zakeeruddin, S. M.; Grätzel, M. *Science* **2011**, *334*, 629−634.
(8) Imahori, H.; Kang, S.; Hayashi, H.; Haruta, M.; Kurata, H.; Isoda, S.; Canton, S. E.; Infahsaeng, Y.; Kathiravan, A.; Pascher, T.; et al. *J. Phys. Chem. A* **2011**, *115*, 3679−3690.
(9) Wang, C.-L.; Chang, Y.-C.; Lan, C.-M.; Lo, C.-F.; Diau, E. W.-G.; Lin, C.-Y. *Energy Environ. Sci.* **2011**, *4*, 1788−1795.
(10) Chang, Y.-C.; Wang, C.-L.; Pan, T.-Y.; Hong, S.-H.; Lan, C.-M.; Kuo, H.-H.; Lo, C.-F.; Hsu, H.-Y.; Lin, C.-Y.; Diau, E. W.-G. *Chem. Commun.* **2011**, *47*, 8910−8912.
(11) Davis, N. K. S.; Thompson, A. L.; Anderson, H. L. *Org. Lett.* **2010**, *12*, 2124−2127.
(12) Imahori, H.; Matsubara, Y.; Iijima, H.; Umeyama, T.; Matano, Y.; Ito, S.; Niemi, M.; Tkachenko, N. V.; Lemmetyinen, H. *J. Phys. Chem. C* **2010**, *114*, 10656−10665.
(13) Lo, C.-F.; Hsu, S.-J.; Wang, C.-L.; Cheng, Y.-H.; Lu, H.-P.; Diau, E. W.-G.; Lin, C.-Y. *J. Phy. Chem. C* **2010**, *114*, 12018−12023.
(14) Kira, A.; Matsubara, Y.; Iijima, H.; Umeyama, T.; Matano, Y.; Ito, S.; Niemi, M.; Tkachenko, N. V.; Lemmetyinen, H.; Imahori, H. *J. Phys. Chem. C* **2010**, *114*, 11293−11304.
(15) Luo, L.; Lin, C.-J.; Hung, C.-S.; Lo, C.-F.; Lin, C.-Y.; Diau, E. W.-G. *Phys. Chem. Chem. Phys.* **2010**, *12*, 12973−12977.
(16) Bessho, T.; Zakeeruddin, S. M.; Yeh, C.-Y.; Diau, E. W.-G.; Grätzel, M. *Angew. Chem., Int. Ed.* **2010**, *49*, 6646−6649.
(17) Fortage, J.; Boixel, J.; Blart, E.; Becker, H. C.; Odobel, F. *Inorg. Chem.* **2009**, *48*, 518−526.
(18) Lin, C.-Y.; Lo, C.-F.; Luo, L.; Lu, H.-P.; Hung, C.-S.; Diau, E. W.-G. *J. Phys. Chem. C* **2009**, *113*, 755−764.
(19) Liu, Y.; Xiang, N.; Feng, X.; Shen, P.; Zhou, W.; Weng, C.; Zhao, B.; Tan, S. *Chem. Commun.* **2009**, 2499−2501.
(20) Imahori, H.; Hayashi, S.; Hayashi, H.; Oguro, A.; Eu, S.; Umeyama, T.; Matano, Y. *J. Phys. Chem. C* **2009**, *113*, 18406−18413.
(21) Lee, C.-W.; Lu, H.-P.; Lan, C.-M.; Huang, Y.-L.; Liang, Y.-R.; Yen, W.-N.; Liu, Y.-C.; Lin, Y.-S.; Diau, E. W.-G.; Yeh, C.-Y. *Chem.-Eur. J.* **2009**, *15*, 1403−1412.
(22) Lu, H.-P.; Tsai, C.-Y.; Yen, W.-N.; Hsieh, C.-P.; Lee, C.-W.; Yeh, C.-Y.; Diau, E. W.-G. *J. Phys. Chem. C* **2009**, *113*, 20990−20997.
(23) Lee, C. Y.; Hupp, J. T. *Langmuir* **2009**, *26*, 3760−3765.
(24) Lin, C.-Y.; Wang, Y.-C.; Hsu, S.-J.; Lo, C.-F.; Diau, E. W.-G. *J. Phys. Chem. C* **2009**, *114*, 687−693.
(25) Rochford, J.; Galoppini, E. *Langmuir* **2008**, *24*, 5366−5374.
(26) Wang, X.-F.; Koyama, Y.; Nagae, H.; Wada, Y.; Sasaki, S.-i.; Tamiaki, H. *J. Phys. Chem. C* **2008**, *112*, 4418−4426.
(27) Eu, S.; Hayashi, S.; Umeyama, T.; Oguro, A.; Kawasaki, M.; Kadota, N.; Matano, Y.; Imahori, H. *J. Phys. Chem. C* **2007**, *111*, 3528−3537.
(28) Tanaka, M.; Hayashi, S.; Eu, S.; Umeyama, T.; Matano, Y.; Imahori, H. *Chem. Commun.* **2007**, 2069−2071.
(29) Campbell, W. M.; Jolley, K. W.; Wagner, P.; Wagner, K.; Walsh, P. J.; Gordon, K. C.; Schmidt-Mende, L.; Nazeeruddin, M. K.; Wang, Q.; Grätzel, M.; et al. *J. Phys. Chem. C* **2007**, *111*, 11760−11762.
(30) Stromberg, J. R.; Marton, A.; Kee, H. L.; Kirmaier, C.; Diers, J. R.; Muthiah, C.; Taniguchi, M.; Lindsey, J. S.; Bocian, D. F.; Meyer, G. J.; et al. *J. Phys. Chem. C* **2007**, *111*, 15464−15478.
(31) Huijser, A.; Marek, P. L.; Savenije, T. J.; Siebbeles, L. D. A.; Scherer, T.; Hauschild, R.; Szmytkowski, J.; Kalt, H.; Hahn, H.; Balaban, T. S. *J. Phys. Chem. C* **2007**, *111*, 11726−11733.
(32) Wiberg, J.; Guo, L.; Pettersson, K.; Nilsson, D.; Ljungdahl, T.; Martensson, J.; Albinsson, B. *J. Am. Chem. Soc.* **2007**, *129*, 155−163.
(33) Rochford, J.; Chu, D.; Hagfeldt, A.; Galoppini, E. *J. Am. Chem. Soc.* **2007**, *129*, 4655−4665.
(34) Zhu, Y.; Zhou, S.; Kan, Y.; Su, Z. *Int. J. Quantum Chem.* **2007**, *107*, 1614−1623.
(35) Chinnasamy, M.; Taniguchi, M.; Izabela, H.-J. K.; Hooi, S.; Kee, L.; Holten, D.; Bocian, D. F.; Lindsey, J. S. *Photochem. Photobiol.* **2007**, *83*, 1513−1528.
(36) Giribabu, L.; Kumar, C. V.; Reddy, P. Y. *J. Porphyrins Phthalocyanines* **2006**, *10*, 1007−1016.
(37) Imahori, H.; Hayashi, S.; Umeyama, T.; Eu, S.; Oguro, A.; Kang, S.; Matano, Y.; Shishido, T.; Ngamsinlapasathian, S.; Yoshikawa, S. *Langmuir* **2006**, *22*, 11405−11411.
(38) Vilmercati, P.; Cudia, C. C.; Larciprete, R.; Cepek, C.; Zampieri, G.; Sangaletti, L.; Pagliara, S.; Verdini, A.; Cossaro, A.; Floreano, L.; et al. *Surf. Sci.* **2006**, *600*, 4018−4023.
(39) Lo, C.-F.; Luo, L.; Diau, E. W.-G.; Chang, I.-J.; Lin, C.-Y. *Chem. Commun.* **2006**, 1430−1432.
(40) Clifford, J. N.; Forneli, A.; Chen, H.; Torres, T.; Tan, S.; Palomares, E. *J. Mater. Chem.* **2011**, *21*, 1693−1696.
(41) Wang, X.; Yang, Y.; Fan, R.; Jiang, Z. *New J. Chem.* **2011**, *34*, 2599−2604.
(42) Imahori, H.; Umeyama, T.; Ito, S. *Acc. Chem. Res.* **2009**, *42*, 1809−1818.
(43) Eu, S.; Hayashi, S.; Umeyama, T.; Matano, Y.; Araki, Y.; Imahori, H. *J. Phys. Chem. C* **2008**, *112*, 4396−4405.
(44) Eu, S.; Katoh, T.; Umeyama, T.; Matano, Y.; Imahori, H. *Dalton Trans.* **2008**, 5476−5483.
(45) Wang, M.; Li, X.; Lin, H.; Pechy, P.; Zakeeruddin, S. M.; Grätzel, M. *Dalton Trans.* **2009**, 10015−10020.
(46) Halme, J.; Vahermaa, P.; Miettunen, K.; Lund, P. *Adv. Mater.* **2010**, *22*, E210−E234.
(47) Gilles, U.; Raymond, Z.; Anthony, H. *Angew. Chem., Int. Ed.* **2008**, *47*, 1184−1201.
(48) Loudet, A.; Burgess, K. *Chem. Rev.* **2007**, *107*, 4891−4932.
(49) Erten-Ela, S.; Yilmaz, M. D.; Icli, B.; Dede, Y.; Icli, S.; Akkaya, E. U. *Org. Lett.* **2008**, *10*, 3299−3302.
(50) Donuru, V. R.; Vegesna, G. K.; Velayudham, S.; Green, S.; Liu, H. *Chem. Mater.* **2009**, *21*, 2130−2138.
(51) Forgie, J. C.; Skabara, P. J.; Stibor, I.; Vilela, F.; Vobecka, Z. *Chem. Mater.* **2009**, *21*, 1784−1786.
(52) Harriman, A.; Izzet, G.; Ziessel, R. *J. Am. Chem. Soc.* **2006**, *128*, 10868−10875.
(53) Sheldrick, G. M. *Acta Crystallogr.* **2008**, *A64*, 112.
(54) Pang, X.-Y.; Gong, F. *E-J. Chem.* **2008**, *5*, 802−809.
(55) Rudzinski, W.; Plazinski, W. *Environ. Sci. Technol.* **2008**, *42*, 2470−2475.
(56) Azizian, S.; Bashiri, H. *Langmuir* **2008**, *24*, 13013−13018.
(57) Zhong, Y.; Si, L.; He, H.; Sykes, A. G. *Dalton Trans.* **2011**, *40*, 11389−11395.
(58) Cui, A.; Peng, X.; Fan, J.; Chen, X.; Wu, Y.; Guo, B. *J. Photochem. Photobiol., A: Chem.* **2007**, *186*, 85−92.
(59) Kumaresan, D.; Thummel, R. P.; Bura, T.; Ulrich, G.; Ziessel, R. *Chem.-Eur. J.* **2009**, *15*, 6335−6339.
(60) Lakowicz, J. R. *Principles of Fluorescence Spectroscopy*, 3rd ed.; Springer: New York, 2006.
(61) Hardin, B. E.; Hoke, E. T.; Armstrong, P. B.; Yum, J.-H.; Comte, P.; Torres, T.; Frechet, J. M. J.; Nazeeruddin, M. K.; Gräetzel, M.; McGehee, M. D. *Nat. Photonics* **2009**, *3*, 406−411.
(62) Yum, J.-H.; Hardin, B. E.; Moon, S.-J.; Baranoff, E.; Nuesch, F.; McGehee, M. D.; Grätzel, M.; Nazeeruddin, M. K. *Angew. Chem., Int. Ed.* **2009**, *48*, 9277−9280.

(63) Hardin, B. E.; Sellinger, A.; Moehl, T.; Humphry-Baker, R.; Moser, J.-E.; Wang, P.; Zakeeruddin, S. M.; Grätzel, M.; McGehee, M. D. *J. Am. Chem. Soc.* **2011**, *133*, 10662−10667.
(64) Hardin, B. E.; Yum, J.-H.; Hoke, E. T.; Jun, Y. C.; Pechy, P.; Torres, T.; Brongersma, M. L.; Nazeeruddin, M. K.; Grätzel, M.; McGehee, M. D. *Nano Lett.* **2010**, *10*, 3077−3083.
(65) Yum, J.-H.; Baranoff, E.; Hardin, B. E.; Hoke, E. T.; McGehee, M. D.; Nuesch, F.; Grätzel, M.; Nazeeruddin, M. K. *Energy Environ. Sci.* **2010**, *3*, 434−437.
(66) Hoke, E. T.; Hardin, B. E.; McGehee, M. D. *Opt. Express* **2010**, *18*, 3893−3904.
(67) Brown, M. D.; Parkinson, P.; Torres, T.; Miura, H.; Herz, L. M.; Snaith, H. J. *J. Phys. Chem. C* **2011**, *115*, 23204−23208.
(68) Hesse, H. C.; Weickert, J.; Hundschell, C.; Feng, X.; Muellen, K.; Nickel, B.; Mozer, A. J.; Schmidt-Mende, L. *Adv. Energy Mater.* **2011**, *1*, 861−869.
(69) Yum, J.-H.; Hardin, B. E.; Hoke, E. T.; Baranoff, E.; Zakeeruddin, S. M.; Nazeeruddin, M. K.; Torres, T.; McGehee, M. D.; Grätzel, M. *ChemPhysChem* **2011**, *12*, 657−661.
(70) Brown, M. D.; Parkinson, P.; Torres, T.; Miura, H.; Herz, L. M.; Snaith, H. J. *J. Phys. Chem. C* **2011**, *115*, 23204−23208.
(71) Humphry-Baker, N.; Driscoll, K.; Rao, A.; Torres, T.; Snaith, H. J.; Friend, R. H. *Nano Lett.* **2012**, *12*, 634−639.
(72) Barea, E. M.; Zafer, C.; Gultekin, B.; Aydin, B.; Koyuncu, S.; Icli, S.; Santiago, F. F.; Bisquert, J. *J. Phys. Chem. C* **2010**, *114*, 19840−19848.
(73) Li, T. C.; Goes, M. S.; Fabregat-Santiago, F.; Bisquert, J.; Bueno, P. R.; Prasittichai, C.; Hupp, J. T.; Marks, T. J. *J. Phys. Chem. C* **2009**, *113*, 18385−18390.
(74) Bisquert, J.; Mora-Sero, I. *J. Phys. Chem. Lett.* **2009**, *1*, 450−456.
(75) Fabregat-Santiago, F.; Barea, E. M.; Bisquert, J.; Mor, G. K.; Shankar, K.; Grimes, C. A. *J. Am. Chem. Soc.* **2008**, *130*, 11312−11316.
(76) Mora-Sero, I.; Bisquert, J.; Fabregat-Santiago, F.; Garcia-Belmonte, G.; Zoppi, G.; Durose, K.; Proskuryakov, Y.; Oja, I.; Belaidi, A.; Dittrich, T.; et al. *Nano Lett.* **2006**, *6*, 640−650.
(77) Mora-Sero, I.; Dittrich, T.; Belaidi, A.; Garcia-Belmonte, G.; Bisquert, J. *J. Phys. Chem. B* **2005**, *109*, 14932−14938.
(78) Liberatore, M.; Burtone, L.; Brown, T. M.; Reale, A.; Carlo, A. D.; Decker, F. *Appl. Phys. Lett.* **2009**, *94*, 173113.